Building a better snail: Lubrication and adhesive locomotion

Brian Chan
Hatsopoulos Microfluids Laboratory, Department of Mechanical Engineering, Massachusetts Institute of Technology, Cambridge, Massachusetts 02139

N. J. Balmforth
Departments of Mathematics and Earth and Ocean Science, University of British Columbia, Vancouver, British Columbia V6T 1Z2, Canada

A. E. Hosoi
Hatsopoulos Microfluids Laboratory, Department of Mechanical Engineering, Massachusetts Institute of Technology, Cambridge, Massachusetts 02139

(Received 17 March 2005; accepted 8 September 2005; published online 28 November 2005)

Many gastropods, such as slugs and snails, crawl via an unusual mechanism known as adhesive locomotion. We investigate this method of propulsion using two mathematical models: one for direct waves and one for retrograde waves. We then test the effectiveness of both proposed mechanisms by constructing two mechanical crawlers. Each crawler uses a different mechanical strategy to move on a thin layer of viscous fluid. The first uses a flexible flapping sheet to generate lubrication pressures in a Newtonian fluid, which in turn propel the mechanical snail. The second generates a wave of compression on a layer of Laponite, a non-Newtonian, finite-yield stress fluid with characteristics similar to those of snail mucus. This second design can climb smooth vertical walls and perform an inverted traverse. © *2005 American Institute of Physics*.
[DOI: 10.1063/1.2102927]

I. INTRODUCTION

Understanding adhesive locomotion, the crawling mechanism adopted by most marine and terrestrial gastropods provides an interesting challenge for fluid dynamicists, biologists, and roboticists alike. As a snail propels itself forward, the forces created by muscles in the foot interact with the substrate through a layer of viscous fluid (pedal mucus) secreted by the animal. Locomotion is directly coupled to the stresses generated within this thin film and the dynamic and material properties of the fluid are intimately involved in the propulsion mechanism.

It has long been known that muscles along the foot of a snail drive deformations that propel the animal forward. Observations of crawling snails show that the moving foot is divided into alternating bands of translating waves and interwaves (see Fig. 1). These waves have been classified by Vlés[1] as direct waves, propagating in the direction of motion of the snail, or retrograde waves, propagating opposite to the snail motion. Rarer forms of movement have also been observed, including diagonal waves, "crawl-step" events,[2] and "galloping," in which the snail lifts a portion of its body off the substrate, similar to an inchworm. However, simple direct or retrograde waves predominate in most species; direct waves are used primarily by terrestrial gastropods while retrograde waves are seen mainly in marine species. It has been well established, by measuring the distance between marked points on the foot[3] or by anatomical evidence obtained by flash-freezing crawling snails,[2,4] that these waves correspond to regions of lateral compression in the foot.

It was not until Lissmann's work in 1946[5] that biologists began to uncover the mechanical role of these waves in driving propulsion. Lissman proposed that there are a number of forces involved in snail locomotion, including what he termed "external sliding friction" in the form of both "drag" and "slip." He recognized that differential friction between the foot and the ground in the wave, and the interwave segments is required to propel the animal forward. However, Lissmann also postulated that the distinct friction within each segment is a result of the snail lifting portions of its foot, creating a thicker mucus layer in the wave regions. While this differential friction is indeed necessary for locomotion, subsequent studies have shown that the difference does not arise from geometrical changes in the interstitial thickness, rather from the unusual properties of the pedal mucus.

The first person to correctly elucidate the role of the pedal mucus in locomotion was Denny,[6] who characterized the properties of the mucus of the banana slug, *Ariolimax columbianus*. He measured a finite yield stress in the fluid and proposed that the requisite differential friction arises naturally if the applied stresses within the mucus in the interwave region remain below the critical yield stress (thus the fluid acts as an adhesive) while stresses in the wave region are sufficient to drive a flow. He then quantitatively compared experimentally measured stresses in pedal mucus under crawling snails with order of magnitude estimates based on measured yield stresses of the fluid.[4] In Sec. II B we expand on Denny's work and present a detailed model of the stresses generated within the mucus.

In addition to stimulating purely academic interest, adhesive locomotion is inspiring a new paradigm in robotics. Robotic design frequently looks to biology to gain insight into the mechanics of locomotion. One can easily argue that

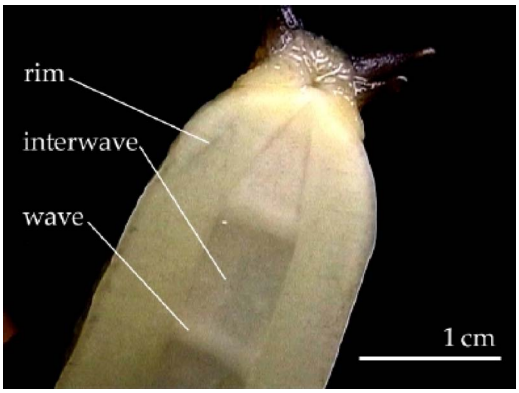

FIG. 1. (Color online). Photograph of the underside of *Limax maximus*, commonly known as the giant leopard slug, showing wave and interwave segments. Waves propagate in the direction of locomotion, i.e., locomotion is driven by direct waves.

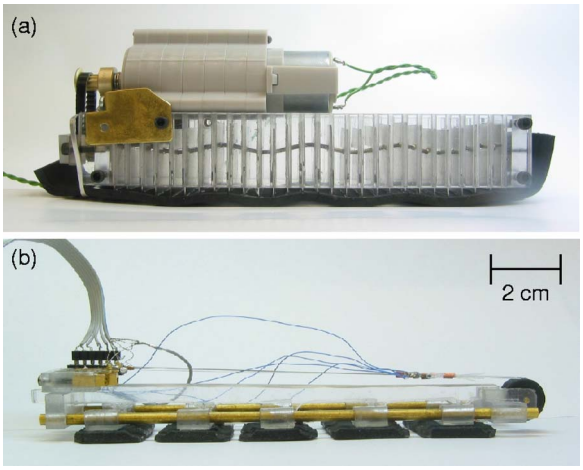

FIG. 2. (Color online). Photograph of two prototype mechanical crawlers. (a) Retrograde crawler (details in Sec. III A). (b) Direct crawler (details in Sec. III B). The direct crawling device is capable of climbing a vertical wall and performing an inverted traverse.

snail locomotion is slow, slimy, and inefficient and hence hardly something roboticists should strive to emulate. However, despite these shortcomings, adhesive locomotion presents two unique advantages. First, gastropods have only one foot so they are mechanically simple and very stable, making mechanical replication far simpler than that required for higher-order organisms. Second, they are often found in habitats that are topologically complex; thus they have evolved means of maneuvering through these challenging terrains by adhering to substrates, enabling them to crawl straight up vertical walls and traverse ceilings and overhangs. This versatility, in conjunction with new soft actuators and other recent technological developments in material science, is beginning to redirect robotic designs toward compliant machines and crawlers.

In light of these advantages, a few research groups have designed and constructed mechanical "snails." Notably, Ito *et al.* have built a mechanical "snail" that consists of a series of electromagnets beneath a soft matrix.[7] A layer of viscous fluid is deposited on the soft substrate and a rigid "snail" is placed on top of the fluid. The magnets then are activated in sequence, creating an out-of-plane wave in the substrate that in turn drives the crawler. However, this design is not ideal, as it is not the "snail" that generates the waves, rather the substrate. More recently, Mahadevan *et al.*[8] carried out a series of experiments using soft hydrogel crawlers to investigate the origin of various crawling gaits. Forward motion in their experiments arises due to differential friction supplied by angled incisions in the gel. However, as in Ito's setup, the substrate provides the propulsive energy rather than the crawler, in this case through externally supplied vibrations.

In this paper, we pursue two paths in analyzing gastropod locomotion. First, we construct a mathematical model that describes the thin fluid layer between the foot and the substrate and demonstrates that, under certain conditions, the stresses in this layer can lead to locomotion. Two separate analyses are carried out for the case of retrograde and direct waves, respectively. Second, to verify the effectiveness of our proposed propulsion systems, we build two mechanical snails, as depicted in Fig. 2: one using direct waves and one using retrograde waves. The direct wave crawler replicates much of the versatility exhibited by live snails and is capable of climbing vertical planes and crawling in an inverted position. The performance of both mechanical snails is compared with model predictions.

II. PROPOSED MECHANISMS AND MATHEMATICAL MODELS

A. Retrograde waves

Locomotion via retrograde waves can be simply induced by out-of-plane waves generated on the underside of the foot. It is likely that, should marine snails crawl via the retrograde mechanism described herein, it would be used in conjunction with an adhesive type of locomotion similar to that described in Sec. II B. However, the retrograde mode proposed in this section can be used exclusively in developing mechanical crawlers, as described in Sec. III A, and the analysis simplifies considerably if we consider the two mechanisms separately. The propulsive power from this type of wave is generated in a manner analogous to a peristaltic pump and the physical mechanism can be simply understood as follows. As the lowest point in the wave ([A] in Fig. 3), moves backward, viscous fluid to the left of the wave is squeezed into a narrow gap, resulting in a local increase in pressure. Conversely, at the back of the wave, fluid flows

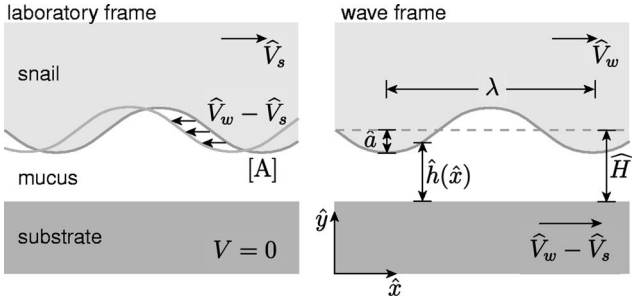

FIG. 3. Schematic illustration of out-of-plane waves, in the laboratory frame, and in the wave frame, generated in a retrograde crawler.

unobstructed into a widening gap, resulting in a decrease in pressure. These two pressures, acting normal to the interface, result in a net force opposite to the direction of wave propagation.

To calculate the velocity of the snail, we first move into a reference frame moving with the wave such that $\hat{h}=\hat{h}(\hat{x})$, i.e., the shape of the foot is no longer time dependent (see Fig. 3). We consider a two-dimensional crawler that is periodic in $\hat{x}$. Here $\hat{V}_s$ is the snail velocity as measured in the lab frame and $\hat{V}_w$ is the wave velocity as measured in the snail frame. Ultimately we would like to answer the following question: Given a motor that can drive a deflection at speed $\hat{V}_w$ in the mechanical foot, how fast will the "snail" go? Unlike the direct wave mechanism described in Sec. II B, the simplest retrograde crawler can operate on a Newtonian fluid that we will assume in our model. If the average gap thickness, $\hat{H}$, is much smaller than the wavelength, λ, we can use a standard lubrication approximation (e.g., Ref. 14) to model the interstitial fluid. The conservation of momentum in the $\hat{x}$ and $\hat{y}$ directions are given by

$$\frac{\partial \hat{p}}{\partial \hat{x}} = \mu \frac{\partial^2 \hat{u}}{\partial \hat{y}^2}, \quad \frac{\partial \hat{p}}{\partial \hat{y}} = 0, \tag{1}$$

where $\hat{p}$ is pressure, μ is the viscosity, $\hat{u}$ is the velocity in the $\hat{x}$ direction, and overcarets denote dimensional quantities. Here we have also restricted our analysis to the limit of small Reynolds number (as is appropriate for snails). Rescaling the variables as follows: $\hat{x}=\lambda x$, $\hat{y}=\hat{H}y$, $\hat{u}=\hat{V}_w u$, $\hat{p}=\lambda\mu\hat{V}_w/\hat{H}^2 p$, $\hat{h}=\hat{H}h$, and $\hat{V}_s=\hat{V}_w V_s$, the x-momentum equation becomes

$$\frac{dp}{dx} = \frac{\partial^2 u}{\partial y^2} \tag{2}$$

subject to the boundary conditions $u(0)=1-V_s$ and $u(h)=1$. Integrating twice, we find

$$u(x,y) = \frac{1}{2}\frac{dp}{dx} y(y-h) + V_s\left(\frac{y}{h}-1\right) + 1. \tag{3}$$

At steady state, the volume flux per unit width through a plane normal to the substrate, $Q=\int_0^h u\, dy$, must be constant for all x. Integrating (3) from 0 to h and solving for the pressure gradient, we find

$$\frac{dp}{dx} = \frac{12}{h^3}\left[h\left(1-\frac{1}{2}V_s\right) - Q\right]. \tag{4}$$

Since $h(x)$ is periodic with wavelength 1, $p(1)=p(0)$, which may be used to solve for the unknown constant Q. Specifically,

$$\int_0^1 \frac{dp}{dx} dx = p(1) - p(0) = 0. \tag{5}$$

Integrating (4) over one wavelength, applying condition (5), and solving for Q, we find

$$Q = \left(1-\frac{1}{2}V_s\right)\frac{I_2}{I_3}, \quad \text{where } I_j = \int_0^1 \frac{dx}{h^j}. \tag{6}$$

Hence, given the wave shape, $h(x)$, we can compute the dimensionless flux, Q, which in turn gives us the pressure gradient, dp/dx and the fluid velocity profile, $u(x)$.

Finally, to find the velocity of the snail we perform a force balance on the foot. The traction acting on the foot is $\mathbf{F}=\hat{\boldsymbol{\sigma}}\cdot\hat{\mathbf{n}}$, where $\hat{\boldsymbol{\sigma}}$ is the dimensional fluid stress tensor and $\hat{\mathbf{n}}$ is the unit outward normal to the foot. Integrating over x and applying force balance on the entire snail in the x direction[9–11] to lowest order in $\hat{H}/\lambda$ yields (in dimensionless form)

$$\int_0^1 p\frac{dh}{dx} + \left.\frac{\partial u}{\partial y}\right|_{y=h} dx = 0. \tag{7}$$

Recall that we have already assumed that the snail does not accelerate but travels at a steady velocity, V_s. The first term in the integral represents the pressure forces acting normal to the foot and the second represents viscous drag. Integrating the first term by parts and substituting (4) for dp/dx, we find

$$3QI_2 = (3-2V_s)I_1. \tag{8}$$

Finally, using the expression for Q from (6) and defining a shape function,

$$A \equiv \frac{I_2^2}{I_1 I_3}, \tag{9}$$

we find an expression for the velocity of the snail,

$$V_s = \frac{6(1-A)}{4-3A}. \tag{10}$$

Thus, given the shape of the deformations in the foot, we can predict the velocity of the animal.

It is straightforward to modify the above calculation to include an inclined substrate and determine whether our mechanical snail is capable of climbing a near-vertical wall. Adding the gravitational body force into Eq. (7), we find

$$-W\sin\phi = \int_0^1 p\frac{dh}{dx} + \left.\frac{\partial u}{\partial y}\right|_{y=h} dx, \tag{11}$$

where ϕ is the angle of inclination measured from the horizontal, $W=\hat{H}mg/\mu\hat{V}_w\lambda b$ is a dimensionless weight parameter, g is gravity, m is the mass of the crawler, and b is the width of the crawler in the z direction. Solving for the snail velocity, we find

$$V_s = \frac{6(1-A)}{4-3A} - \frac{W\sin\phi}{I_1(4-3A)}. \tag{12}$$

Thus the tangential force balance indicates that the snail can crawl up any surface, provided $6(1-A) > W/I_1$. However, it is important to note that the normal force balance limits our snail's climbing capabilities to inclinations of $\phi < \pi/2$ i.e., the crawler cannot traverse an overhang nor can it crawl up a truly vertical surface. Since there is no normal force adhering the crawler to the substrate, it cannot retain contact with a

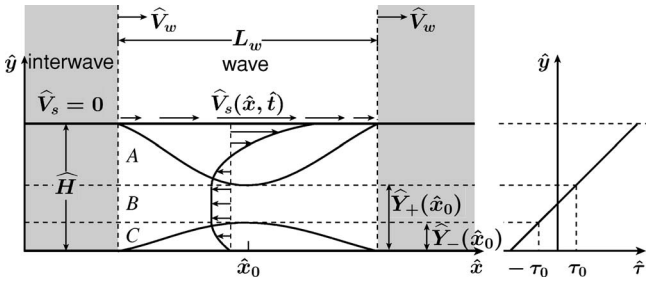

FIG. 4. Schematic illustration of the interstitial fluid of a direct wave crawler with $\hat{y}$ vs the xy component of stress, $\hat{\tau}$, plotted on the right.

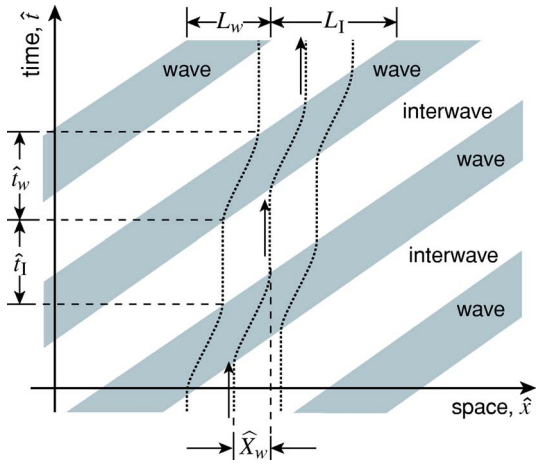

FIG. 5. A space–time plane showing the progression of the contraction waves and interwaves as they sweep along the snail's foot. The crooked, roughly vertical dotted lines denote the world lines of material points on the foot. The lengths of the contraction wave and interwave, L_w and L_I, respectively, are indicated, as are the time intervals that each material foot point spends in each ($\hat{t}_w$ and $\hat{t}_I$, respectively). The displacement incurred after the passage of each contraction wave is $\hat{X}_w$, as illustrated.

vertical wall, in contrast to the adhesive mechanism described in the next section.

B. Direct waves

Adhesive locomotion via direct waves was first correctly described by Denny[4,6] in an article in which he answers the thought-provoking question "How can an animal with only one foot walk on glue?" The analogy of a kink propagating across a carpet, often used to describe the motion of dislocations, is equally apt here. To propel itself forward, the snail uses its muscles to initiate a small region of compression at the tail (the "kink"). This compressed region then travels from the tail to the head along the foot (the "carpet"). When it reaches the head, the snail once more extends to its full length, shifting the entire animal forward.[12,13]

Denny[4] correctly postulated that this mode of locomotion requires that the forces generated by the moving portion of the foot must be offset by the adhesive forces under the interwave portions stating "a gastropod will move forward if the *reactive force* beneath the stationary parts of the foot (the interwaves) is sufficient to offset the *frictional force* due to the movement of the waves and the rim." That is if the adhesive forces do not exceed the shear forces, the entire snail will simply slip backward as the wave propagates forward, resulting in no net translation. Denny also correctly identified the source of this differential friction, arguing that the muscles in a snail are not strong enough to lift the foot and generate a variable gap thickness, therefore the difference must result from a change in the properties of the pedal mucus in the wave and interwave regions. This change is reflected in the finite yield stress of the mucus. In regions where the foot is shearing the fluid sufficiently, namely the wave regions, the applied stress exceeds the critical yield stress and drives a flow; in the interwave regions, the fluid does not yield, effectively gluing the foot to the substrate.

To relate the externally applied stresses and the properties of the pedal mucus to locomotion, we first compute the velocities and pressures within the fluid. We consider a flat foot on top of a fluid layer of thickness, $\hat{H}$, with periodically alternating wave and interwave regions (see Fig. 4). As with the retrograde crawler, we restrict our analysis to two dimensions with periodic variations in $\hat{x}$. In the interwave, the fluid is stationary. In the wave region, of length L_w, where the muscles are compressed, the foot drives the upper boundary of the fluid forward with surface velocity $\hat{V}_s(\hat{x},\hat{t})$. The boundary between the wave and interwave moves forward with a velocity $\hat{V}_w$. Note $\hat{V}_w$ and $\hat{V}_s(\hat{x},\hat{t})$ need not be the same velocity and the compatibility condition relating the two to the motion of the snail as a whole can be constructed as follows.

First, we sketch the geometry of the contraction wave on the space–time plane (Fig. 5). The instantaneous velocity of the foot in the contraction wave is fixed in the frame moving with the wave $\hat{V}_s = \hat{V}_s(\hat{x} - \hat{V}_w\hat{t}) \equiv \hat{V}_s(\hat{\xi})$, where $\hat{\xi}$ is the space coordinate in the moving frame. If L_w and L_I denote the lengths of the contraction wave and interwave, then the time taken for the wave and interwave to pass a fixed point of reference are $\hat{t}_w^{\text{fixed}} = L_w/\hat{V}_w$ and $\hat{t}_I = L_I/\hat{V}_w$, respectively. However, a particular material point in the foot prolongs the interval $\hat{t}_w$, it spends in the contraction wave as a result of its own motion, i.e., $\hat{t}_w > \hat{t}_w^{\text{fixed}}$. Over this extended interval, the point on the foot jumps a total distance $\hat{X}_w$. Consequently, the snail speed must be given by

$$\hat{V}_{\text{snail}} = \frac{\hat{X}_w}{\hat{t}_w + \hat{t}_I}, \tag{13}$$

where $\hat{X}_w = \int_0^{\hat{t}_w} \hat{V}_s(\hat{x} - \hat{V}_w\hat{t})\,d\hat{t}$. From Fig. 5 we see that the time interval spent by a point on the foot in the contraction wave is $\hat{t}_w = (L_w + \hat{X}_w)/\hat{V}_w$. Similarly, $\hat{t}_I = L_I/\hat{V}_w$. Hence

$$\hat{V}_{\text{snail}} = \frac{\hat{V}_w\hat{X}_w}{\hat{X}_w + L_w + L_I}. \tag{14}$$

If $\hat{V}_*$ is a characteristic value of $\hat{V}_s(\hat{\xi})$, then $\hat{X}_s \sim \hat{V}_*\hat{t}_w$, and we estimate

$$\hat{V}_{\text{snail}} \sim \frac{\hat{V}_w \hat{V}_*}{\hat{V}_w(1+R) - R\hat{V}_*}, \tag{15}$$

where $R = L_I/L_w$ is the ratio of the size of the interwave segment to the wave segment. As we shall see, this number cannot be arbitrarily changed as L_I must be sufficient to prevent the snail from slipping backward. As expected, the larger the characteristic foot speed, $\hat{V}_*$, the greater the snail speed. For typical land snails, surface velocities are approximately two times faster than the animal.

Returning to the stresses generated in the mucus layer, in the wave region, conservation of momentum of the fluid is given by

$$\hat{\nabla}\hat{p} = \hat{\nabla} \cdot \hat{\boldsymbol{\tau}}, \tag{16}$$

where $\hat{p}$ is the pressure and $\hat{\boldsymbol{\tau}}$ is the deviatoric stress (again overcarets indicate dimensional variables). To model the interstitial fluid, we again assume that $\hat{H}/L_w \ll 1$ and, unlike the retrograde case, this thickness does not vary with $\hat{x}$. Any spatial variations in the flow field are driven by local variations in the surface velocity. We model the mucus as a Herschel–Bulkley fluid, which captures the property of both a finite yield stress and a shear-dependent effective viscosity. Such a fluid, in the lubrication limit, is governed by the following constitutive law, relating the xy component of the stress tensor, $\hat{\tau}$, to the strain rate, $\dot{\gamma} = \partial\hat{u}/\partial\hat{y}$, the yield stress, τ_0, the consistency, μ, and the power law index, n,

$$\hat{\tau} = (\tau_0 + \mu|\dot{\gamma}|^n)\text{sgn}(\dot{\gamma}), \tag{17}$$

when $|\hat{\tau}| \geqslant \tau_0$. If $|\hat{\tau}| < \tau_0$, there is no shear in the layer, namely $\partial\hat{u}/\partial\hat{y} = 0$. Rescaling by $\hat{u} = n/(n+1)\hat{H}(2\tau_0/\mu)^{1/n}u$, $\hat{y} = \hat{H}y$, $\hat{x} = L_w x$, $\hat{p} = L_w/\hat{H}\tau_0 p$, and applying a lubrication approximation as before, we find that the pressure does not vary across the depth, i.e., $\hat{p} = \hat{p}(\hat{x}, \hat{t})$, and that the velocity is governed by one of two relations depending on whether the local stress exceeds the yield stress of the fluid;

$$|\hat{\tau}| \geqslant \tau_0: \quad \frac{\partial p}{\partial x} = \frac{\partial}{\partial y}\left[\left(1 + 2\left|\frac{n}{n+1}\frac{\partial u}{\partial y}\right|^n\right)\text{sgn}(\dot{\gamma})\right], \tag{18}$$

$$|\hat{\tau}| < \tau_0: \quad \frac{\partial u}{\partial y} = 0, \tag{19}$$

where we have neglected terms of order $\hat{H}/L_w$ and higher.

Since the fluid is incompressible and the thickness of the layer does not change, the net flux through any cross section perpendicular to the foot must be the same at any position, x. In the interwave regions, this flux is zero since the fluid is stationary. Therefore, the net flux in the wave region must also be zero. This is only possible if there exists a positive pressure gradient within each wave segment that pushes fluid backward somewhere in the layer as the foot drags fluid near the top forward. Thus the velocity profile can be divided into three parts, as shown in Fig. 4: region A at the top ($\hat{Y}_+ < \hat{y} \leqslant \hat{H}$), where the flow is parabolic (for $n=1$) and pulled forward by the foot; region B ($\hat{Y}_- < \hat{y} \leqslant \hat{Y}_+$) consisting of a backward pseudoplug flow; and region C ($0 \leqslant \hat{y} \leqslant \hat{Y}_-$), again parabolic (for $n=1$), connecting the no-slip boundary condition at the substrate to the backward plug flow. As we shall see, region B is not a true plug flow, as the velocity and the position of the yield surfaces vary slowly with x. Hence we refer to the region as a pseudoplug rather than a true plug.[15]

We now solve for the flow field in each region beginning with A. In this region, $\dot{\gamma} \geqslant 0$ and $|\hat{\tau}| \geqslant \tau_0$. Solving (19) with boundary conditions $u = u_p$ and $\partial u/\partial y = 0$ at $y = Y_+$, we find the velocity, u_A is given by

$$u_A = \left(\frac{1}{2}\frac{dp}{dx}\right)^{1/n}(y - Y_+)^{(n+1)/n} + u_p. \tag{20}$$

In region B, $|\hat{\tau}| < \tau_0$; thus the velocity field is not a function of y. Hence

$$u_B = u_p. \tag{21}$$

In region C, $\dot{\gamma} \leqslant 0$ and $|\hat{\tau}| \geqslant \tau_0$. Applying the boundary conditions $u = u_p$ and $\partial u/\partial y = 0$ at $y = Y_-$ we obtain

$$u_C = \left(\frac{1}{2}\frac{dp}{dx}\right)^{1/n}(Y_- - y)^{(n+1)/n} + u_p. \tag{22}$$

The four unknowns in the system are now dp/dx, u_p (the velocity in the pseudoplug region), and the dimensionless positions of the yield surfaces, Y_+ and Y_-. To solve for these unknowns we apply conservation of mass, boundary conditions at $y=1$ and $y=0$ (which have not yet been enforced), and a yield condition. Applying the boundary conditions $u(y=0) = 0$ and $u(y=1) = V_s$ we find our first two conditions

$$\left(\frac{1}{2}\frac{dp}{dx}\right)^{1/n} Y_-^{(n+1)/n} + u_p = 0, \tag{23}$$

$$\left(\frac{1}{2}\frac{dp}{dx}\right)^{1/n}(1 - Y_+)^{(n+1)/n} + u_p = V_s, \tag{24}$$

where V_s is the dimensionless surface velocity. If the dimensional surface velocity is written as $\hat{V}_s = V_0 f(\hat{x}, \hat{t})$, where V_0 is the maximum surface velocity in the wave region; then

$$V_s = f\frac{n+1}{n}\left(\frac{V_0^n \mu}{2\tau_0 \hat{H}^n}\right)^{1/n} \equiv \frac{n+1}{n}B_n^{-1/n} f, \tag{25}$$

where B_n is the Bingham number and represents a dimensionless yield stress.

By conservation of mass we know that the total flux Q, through a surface perpendicular to the foot, must be zero. In the wave, $Q = Q_A + Q_B + Q_C = 0$, where Q_i is the flux in region i. Integrating Eqs. (20)–(22) in y and rearranging, we find our third condition

$$Y_-^{(n+1)/n} = \frac{n}{2n+1}[(1 - Y_+)^{(2n+1)/n} + Y_-^{(2n+1)/n}]. \tag{26}$$

Finally, $\hat{\tau}$ is a linear function of height with slope $d\hat{p}/d\hat{x}$. Considering the slope of the line in the stress plot in Fig. 4, we find our final yield condition $d\hat{p}/d\hat{x} = 2\tau_0/\hat{h}_p$, where $\hat{h}_p = \hat{Y}_+ - \hat{Y}_-$, is the dimensional thickness of the plug region, or in dimensionless form,

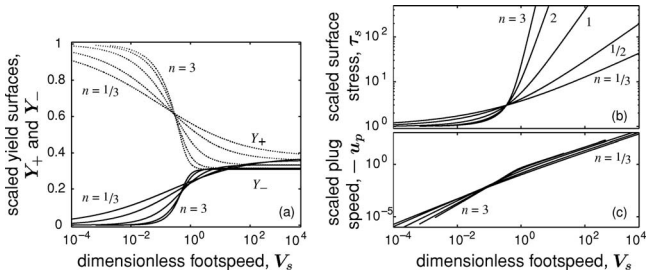

FIG. 6. The scaled pseudoplug velocity, u_p, surface stress, τ_s, and the yield surfaces, Y_+ and Y_-, as functions of the dimensionless surface velocity, V_s, for power law indices of $n=1/3$, $1/2$, 1, and 2.

$$\frac{dp}{dx}(Y_+ - Y_-) = 2. \tag{27}$$

Equations (23), (24), (26), and (27) can now be combined to solve for the four unknowns: dp/dx, u_p, Y_+, and Y_-. After some algebra, the system can be reduced to a single transcendental equation for Y_- with the dimensionless surface velocity (or equivalently, the Bingham number) and the power law exponent as the only remaining parameters:

$$Y_-^{(n+1)/n}\left[\left(\frac{2n+1}{nY_-}-1\right)^{(n+1)/(2n+1)}-1\right] = V_s\left[1-Y_-\left(\frac{2n+1}{nY_-}-1\right)^{n/(2n+1)}-Y_-\right]^{1/n}. \tag{28}$$

The real solutions to this equation as a function of V_s (or equivalently B_n), along with $u_p=-\left(\frac{1}{2}dp/dx\right)^{1/n}Y_-^{(n+1)/n}$, the surface stress, τ_s, and $Y_+=1-Y_-\left[(2n+1)/nY_--1\right]^{n/(2n+1)}$ are all plotted in Fig. 6 for various n. As expected, for large surface velocities (or small yield stress), the yield surfaces come together and the velocity profiles approach the Newtonian parabolic solution. As the surface velocity becomes small (or yield stress becomes large), the majority of the fluid resides in the pseudoplug, moving slowly backward with small shear layers near the top and bottom surfaces.

Now that we have expressions for pressures, yield surfaces, and stresses in terms of the surface velocity, we can return to real space and construct the full solution in the gap. Switching to a frame following the wave, the surface velocity becomes a function of ξ only, i.e., $V_s=(n+1)/nB_n^{-1/n}f(\xi)$. So, within a contraction wave, the surface velocity (dictated by the local foot speed), starts at $V_s=0$ at the one end of the wave and achieves a maximum velocity, $V_s=(n+1)/nB_n^{-1/n}$, somewhere in the middle, then drops back down to $V_s=0$. For example, if $f(\xi)=16\xi^2(1-\xi)^2$, we arrive at the yield surfaces shown in Fig. 7. Note that it is most expeditious to solve for ξ explicitly in terms of Y_-, rather than implicitly solve for all the variables in terms of ξ.

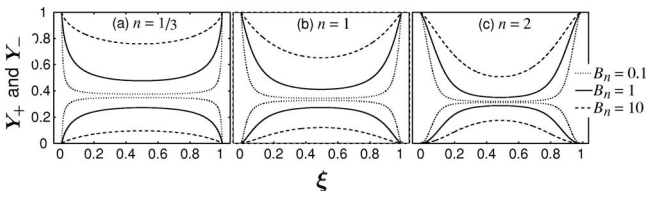

FIG. 7. Yield surfaces in real space for varying B_n and n.

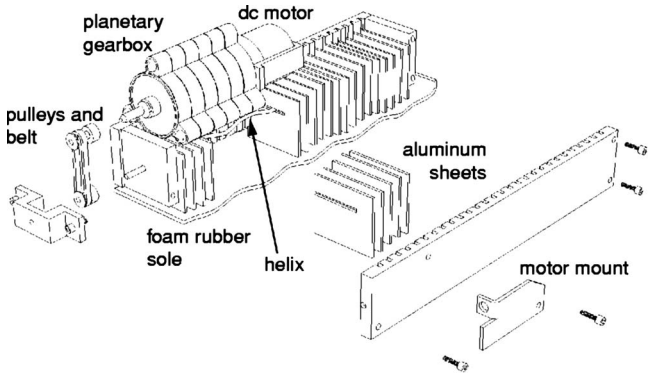

FIG. 8. Design of the retrograde crawler consisting of a shallow spiral threaded through a series of aluminum sheets attached to a rubber foot. The rigid sheets drive a sinusoidal wave in the flexible foot, propelling the crawler forward.

III. DESIGN AND IMPLEMENTATION OF MECHANICAL CRAWLERS

To test the efficacy of these mechanisms, two robotic snails, one retrograde (Robosnail I) and one direct (Robosnail II), were designed and constructed. Unlike previously developed mechanical snails,[7,8] both snails possess self-contained crawling mechanisms and do not require energy input from the substrate. As we shall see, the mechanics of retrograde versus direct crawling is quite different, hence each snail is uniquely suited to quite different environments.

A. Retrograde crawler

Robosnail I, our prototype retrograde crawler, has a solid polycarbonate body, as shown in Fig. 8. The motor, powered by an external dc power source, is capable of supplying 1.5, 3.0, and 4.5 V, and is connected to a variable-speed gearbox. A toothed pulley connects the gearbox to a shallow brass helix that passes through an array of aluminum sheets perforated with slots. Each of the sheets is constrained to vertical motion as they ride in the equally spaced slots along the body. The bottom edges of the aluminum sheets are glued onto a flexible foam sheet. When the helix is spun by the motor and gearbox, it causes the plates to translate up and down inside their tracks in a traveling sinusoidal wave (evident when viewed from the side). As described in Sec. II A, this sinusoidal wave generates regions of high pressure in front of the wave where the fluid is squeezed into a narrow gap, and regions of low pressure behind the wave where the fluid is allowed to expand. These pressures generate forces normal to the interface, driving the snail in the opposite direction of the wave.

A test track slightly larger than the width of the snail, constructed to minimize the leakage of fluid past the open sides of the foot, was filled with a 5 mm thick layer of glycerol and Robosnail I was activated on top of the layer. After the motion reached steady state, measurements of wave speed and snail speed were recorded. The velocities achieved by Robosnail I as a function of wave speed are shown later in

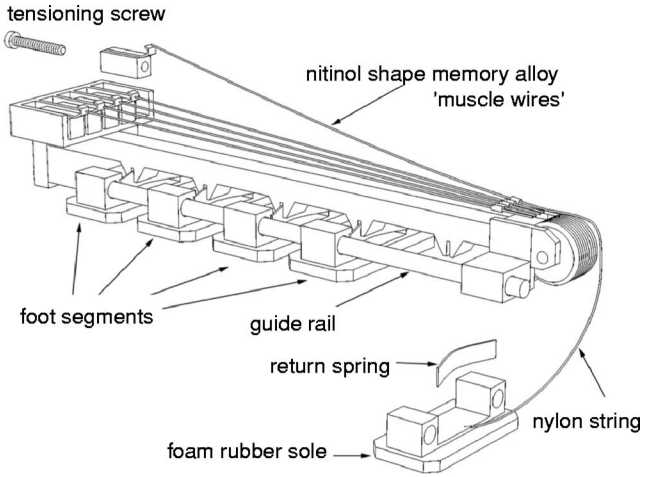

FIG. 9. Design of the direct crawler that uses shape memory alloy wires to activate a compression wave along the underside of the foot.

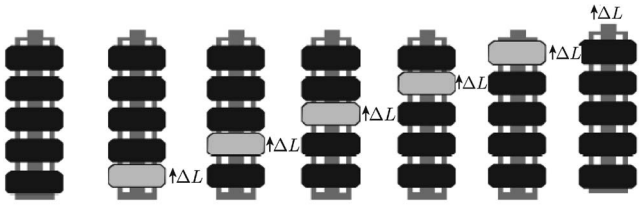

FIG. 10. Activation sequence for the direct crawler.

Fig. 11(b). As predicted, the snail velocity scales linearly with the wave velocity. It is simple to verify that the locomotion is indeed driven by stresses generated within the fluid layer; when the crawler is activated on a dry surface it moves slowly *in the direction of wave propagation* opposite to what is predicted and observed when the fluid layer is present. This simple test underscores the importance of the thin fluid film in the propulsion mechanism.

Taking a best fit of the data in Fig. 11(b), and using Eq. (10) with a sinusoidal wave profile, we predict an average gap thickness of $\hat{H}=(1.9\pm0.1)\hat{a}$, where $\hat{a}=1$ mm. Interstitial heights were not directly measured and, although this estimate is quite reasonable, it is likely that the model slightly overpredicts the gap thicknesses achieved experimentally. Despite the narrow track, there was considerable leakage out the side of the foot as the crawler progressed, reducing the effective pressures within the gap. Hence, we expect the mathematical model to overestimate the speed of the mechanical crawler or equivalently overestimate the gap thickness.

B. Direct wave crawler

Robosnail II was built to mimic the direct wave, adhesive locomotion of land snails. Unlike real snails, which have one continuous foot of muscle, the foot of Robosnail II is made up of five discrete, sliding sections (see Fig. 9). Each of the five sections move forward along a track by a small fixed amount, ΔL, relative to the body. After all five segments have advanced, the body slides forward, returning the segments to their original positions. These small motions occur in sequence, as illustrated in Fig. 10.

The prototype consists of five Nitinol wires attached to nylon cords wrapped 180° around a pulley and tied to five sheets of polycarbonate (see Fig. 9). Each of the sheets is attached to a pair of guides that allow only fore–aft translation. A leaf spring held by the main body returns each of the sheets to its original position when there is no other force present. The springs supply the restoring forces necessary to return the wires to their outstretched positions. The wires are crimped in loops at the ends; one end is tied to the cords controlling the foot, and the other end of each wire is looped around adjustable brass fasteners to allow proper tightening of the wire and cords. It was important for the wires to be correctly tensioned such that the springs succeed in restretching the wires, but not so tight as to limit the motion of the foot segments. The tightness adjustment is achieved by turning the screws through which the wire mounts are threaded.

Laponite[16,17] was used as a lubricating fluid, chosen for its finite yield stress and ready availability. To test the wall climbing ability of Robosnail II, we mounted it on a tiltable platform covered in a 1.5 mm thick layer of Laponite. Since Laponite has a yield stress of 100 Pa, this gives us an approximate Bingham number of $B_n \sim O(1)$, which corresponds to a surface velocity of order $V_s \sim O(1)$. The tilt angle, ϕ, was measured from the horizontal. Here $\phi=\pi/2$ corresponds to a vertical wall; angles greater than $\pi/2$ indicate that the snail crawls up an overhang in an inverted position; $\phi=\pi$ corresponds to a fully inverted traverse. Robosnail II was able to climb the Laponite-coated surface tilted at any angle, including both a vertical and fully inverted position.

Experimental data shows that the motion per cycle is in all cases slightly less than the translation of one foot, $\Delta L=\hat{X}_w$. Ideally, if there is no backward slip, the crawler displacement per cycle, D, should be $\hat{X}_w$. However, data in Fig. 11(a) shows that there is some slippage at all inclinations, with the maximum occurring around $\theta\approx 3\pi/4$ when gravity is working to oppose both the direction of motion and the normal force that contributes to adhesion. At high tilt angles, much of the adhesive force of the Laponite supports both the weight of the snail and the resistance supplied by the interwave sections, while at near-flat angles near 0 and π, the adhesive force is required primarily to resist the friction on the moving foot. Thus, we expect a minimum displacement somewhere between $\pi/2$ and π, as is observed in the experiments, when gravity works to decrease traction and to increase the resistive force of the weight.

The slipping of the stationary sections could be attributed to a number of phenomena. Neither the Laponite layer nor the foam rubber of the crawler's foot sections is perfectly flat and imperfections in the thickness of the Laponite layer could perturb the local stress field driving a flow. Another likely cause for slippage is that the Laponite under the stationary sections may not have had enough time to resolidify. Once the Laponite has yielded, the microstructure reforms gradually, hence the effective yield stress after flowing is less than it was immediately before yielding. Only after a char-

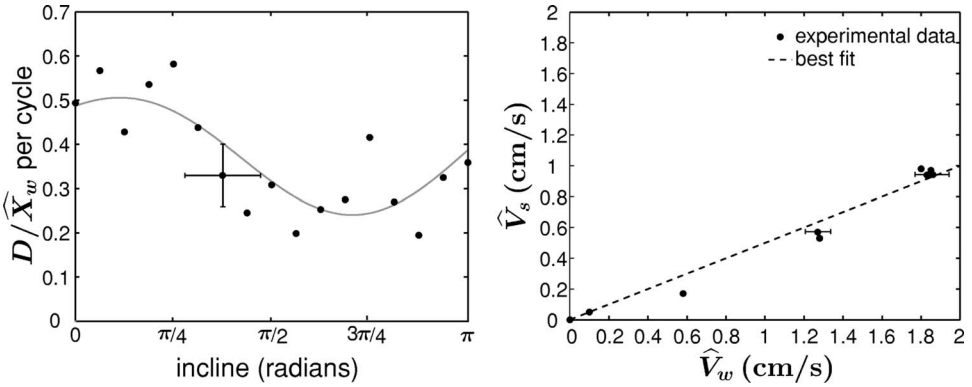

FIG. 11. (a) Experimental data showing slippage of the direct crawler as a function of inclination angle. The y axis indicates a dimensionless displacement, $D/\hat{X}_w$, where $D/\hat{X}_w=1$ corresponds to no slippage. (b) Experimental data of the retrograde snail velocity, $\hat{V}_s$, vs wave velocity, $\hat{V}_w$. As expected, the snail velocity scales linearly with the wave velocity; the slope corresponds to a gap thickness of $\hat{H}=(1.9\pm0.1)\hat{a}$. Characteristic error bars are shown in both plots; vertical error bars are smaller than the symbols in (b).

acteristic "healing" time does the yield stress return to its original value. This last problem can be remedied by increasing the time of each cycle, allowing the Laponite to resolidify at the expense of slowing down the translational speed of the snail. Finally, it was observed that there was delamination of the Laponite layer from the segments of the foot, decreasing the traction of the stationary foot segments.

IV. DISCUSSION

It is clear that the two different crawling mechanisms we have investigated are ideally suited to very different types of terrain. The retrograde crawler that uses peristaltic forces rather than adhesive forces cannot climb vertical walls. However, it has the advantage of being insensitive to the fluid properties and thus can easily maneuver over mud or other mushy surfaces. In contrast, the direct wave crawler can traverse extremely complex topologies including climbing vertical walls and traversing overhangs in an inverted position. The tradeoff for this versatility is that the mechanical crawler has very specific requirements regarding the interstitial fluid properties. In particular, in order to perform these complex maneuvers, the yield stress of the fluid must be sufficient to support the weight of the crawler. The mathematical models discussed in Secs. II A and II B give us some insight as to how to design crawlers to maximize their versatility and minimize the drawbacks outlined above.

A. Exact solutions and optimal wave profiles for the retrograde crawler

The optimization questions that arise in designing retrograde crawlers are primarily geometric. Ideally we would like to know how to change the shape of the deformations in the foot to optimize various quantities such as speed and efficiency. We begin by investigating the limit of both small- and large-amplitude deformations (see Fig. 12).

For small wave amplitudes we consider $h(x)=1+a\delta(x)$, where $\bar{\delta}=0$, and the overbar indicates an x average. Taylor expanding the integrands in (9) we find the shape function A becomes

$$A=\frac{(1+3a^2\overline{\delta^2})^2}{(1+a^2\overline{\delta^2})(1+6a^2\overline{\delta^2})}. \tag{29}$$

This gives, to lowest order, a snail velocity of

$$V_s=6a^2\overline{\delta^2}. \tag{30}$$

Thus, the snail speed is maximized for profiles that make the average of δ^2 as large as possible (recall that the surface velocity, V_s is the same as the snail velocity, V_{snail}, in the retrograde crawler). Square-wave-type profiles accomplish such a maximization while sharp jagged profiles do the worst job.

As the wave amplitude becomes large, the snail foot nearly touches down on the plane beneath and locally, $h\approx h_*+(\partial^2 h_*/\partial x^2)(x-x_*)^2/2$. The I_j integrals then become dominated by local contributions near $x=x_*$ and reduce to derivatives of Lorentzians:

$$I_1\sim\pi\sqrt{\frac{2}{h_*(\partial^2 h_*/\partial x^2)}},\quad I_2\sim\frac{1}{2h_*}I_1,\quad I_3\sim\frac{3}{8h_*^2}I_1. \tag{31}$$

Hence, $A\to 2/3$ and so $V\to 1$. In other words, for any profile with a generic parabolic minimum, when extended near the underlying plane, the foot acts like a caterpillar tread and drives the snail at the wave speed.

In addition to these important limits, there are several special cases for which the crawler velocity can be exactly computed. For a sinusoidal deformation, the integrations in A can be performed analytically. If the gap thickness is given

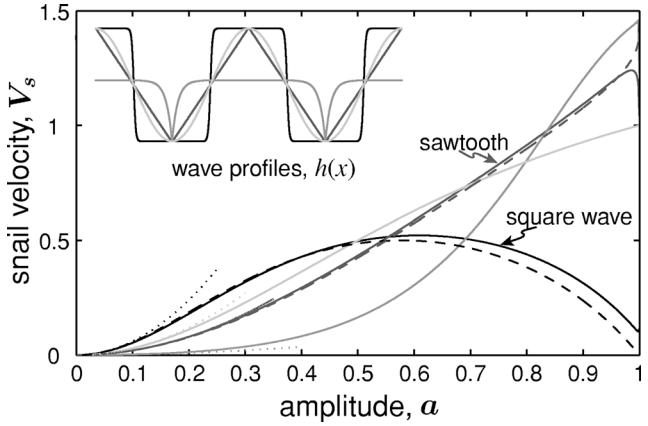

FIG. 12. Dimensionless snail speeds for different wave profiles. The square-wave-like profile is given by $\delta=\tanh 12\cos(2\pi x)$, and the sawtooth-like profile by a Fourier series truncated at 16 terms. The spiky, sharp profile was built using the function $\exp(-6\sqrt{1+\cos 2\pi x})$. The dotted lines show the initial parabolic behavior; the dashed lines show the sawtooth and square wave snail velocity as a function of wave amplitude.

TABLE I. Summary of snail velocities, V_s, and shape functions, A, for various wave profiles. The top two represent generic small and large amplitude waves, respectively; the bottom three are exact solutions for a sinusoidal, square wave, and sawtooth profile. In the sawtooth expressions, $M=\ln[(1+a)/(1-a)]$.

Profile	A	V_s
$h(x)=1+a\delta(x)$	$\approx 1-a^2\overline{\delta^2}$	$\approx 6a^2\overline{\delta^2}$
$h\approx h_*+h_*''(x-x_*)^2/2$	$\to 2/3$	$\to 1$
$h(x)=1-a\cos 2\pi x$	$\dfrac{2}{2+a^2}$	$\dfrac{3a^2}{1+2a^2}$
Square wave	$\dfrac{(1+a^2)^2}{1+3a^2}$	$\dfrac{6a^2(1-a^2)}{1+6a^2-3a^4}$
Sawtooth	$\dfrac{2a}{M}$	$\dfrac{3(M-2a)}{2M-3a}$

by $h(x)=1-a\cos 2\pi x$ in dimensionless form [or equivalently $\hat{h}(\hat{x})=\hat{H}-\hat{a}\cos(2\pi\hat{x}/\lambda)$], the integrals in (9) become $I_1=(1-a^2)^{-1/2}$, $I_2=(1-a^2)^{-3/2}$, and $I_3=(2+a^2)/2(1-a^2)^{5/2}$, resulting in a simple expression for snail speed,

$$V_s=\frac{3a^2}{1+2a^2}. \tag{32}$$

Since the dimensional amplitude of the wave, $\hat{a}$, cannot exceed the average gap thickness, $\hat{H}$, $a\leqslant 1$. Here V_s as a function of a is plotted in Fig. 12. We find that, for a sinusoidal deformation, the snail velocity monotonically approaches the wave speed, i.e., $\hat{V}_s\to\hat{V}_w$, as $\hat{a}\to\hat{H}$.

Two other analytical examples (not necessarily realizable, though) are the square wave and sawtooth, for which

$$I_1=\frac{1}{1-a^2},\quad I_2=\frac{1+a^2}{(1-a^2)^2},\quad I_3=\frac{1+3a^2}{(1-a^2)^3}, \tag{33}$$

and

$$I_1=\frac{1}{2a}\log\left(\frac{1+a}{1-a}\right),\quad I_2=\frac{1}{1-a^2},\quad I_3=\frac{1}{(1-a^2)^2}, \tag{34}$$

respectively. It is easy to see that the square wave does well near $a=0$ since it has a large average of δ^2, but does poorly as $a\to 1$, where the sawtooth is better. A comparison between the sinusoidal, square-wave-like and sawtoothlike profiles is shown in Fig. 12. Also shown is a spiky, sharp profile built using the function $\exp(-6\sqrt{1+\cos 2\pi x})$. Clearly there is a tradeoff between a preference for squarer profiles at low amplitude, to profiles with sharp minima at large amplitude. It is also possible for the snail to be driven faster than the wave for the latter-type profiles. (Note that the smooth profiles swerve sharply near $a=1$ to give the expected result for profiles, with parabolic minima as $a\to 1$.) Obviously, this limit is a bit artificial, since the profile cannot be too sharp without violating the lubrication assumption. Analytic and approximate solutions are summarized in Table I.

We can now also determine if the crawler can climb a near-vertical slope. For a sinusoidal deformation, the snail can climb a wall if $6[1-2/(2+a^2)]>W\sqrt{1-a^2}$. Note that the gravitational sliding can always be dominated by the forward motion if $a\to 1$.

It is also interesting to compare this solution to that obtained by Taylor[18] for a free-swimming undulating sheet. Taylor's sheet, which has fluid on both sides and does not interact with a bounding wall, displays the same scaling with amplitude as $\hat{a}\to 0$, namely $\hat{V}_s\propto\hat{a}^2$. For a periodic wave profile, and a wall parallel to the crawler, we can solve the full biharmonic problem without making the lubrication assumption by decomposing the wave profile into a Fourier series (as in Taylor's article). It is fairly straightforward to show that the first term of the asymptotic series in wave amplitude cannot contribute to driving the snail, and so $V\sim O(a^2)$, wide or narrow fluid layers alike.

B. Optimized design of direct crawlers

In the direct crawler, it is clear that the interwave segments play a critical role in adhesive locomotion. As we have seen, without the resistance provided by the interwave regions, the snail slips backward as the waves move forward resulting in no net translation. Hence the maximum allowed wave speed is directly related to the interwave area. We can now use the relations derived in Sec. II B to design the appropriate ratio of wave and interwave areas in a mechanical crawler given a fluid with known properties (or conversely, given a snail foot, we can calculate the minimum required Bingham number for the fluid). If the adhesive crawler is restricted to a flat surface, the yield stress needed to keep snail from sliding backward is limited by $\tau_0 L_I\geqslant\int_{\text{wave}}\hat{\tau}(\hat{\xi},\hat{H})d\hat{\xi}$, where L_I is the interwave length and the integration is performed along the underside of the foot in the wave region. If the surface velocity is symmetric in $\hat{\xi}$, we can change the integration variable to V_s and write the criterion in dimensionless form as

$$\frac{L_I}{L_w}\geqslant 2B^{1/n}\frac{n}{n+1}\int_0^1\tau_s(V_s)\frac{dV_s}{f'(V_s)}, \tag{35}$$

where, as before, $\hat{V}_s=V_0 f[\xi(V_s)]$. The surface stress, τ_s, in the integrand, is plotted in Fig. 6 or, alternatively, is given by

$$\tau_s(V_s)=1+\left(\frac{n+1}{n}\right)^{2n}\frac{dp}{dx}(1-Y_+). \tag{36}$$

If the crawler is required to climb a vertical wall, this criterion must be modified to include the weight of the crawler, namely, $\tau_0 L_I\geqslant\int_{\text{wave}}\hat{\tau}(\hat{\xi},\hat{H})d\hat{\xi}+mg/Nb$, where m is the mass of the crawler, b is the width, N is the number of wave segments, and g is gravity. In dimensionless form this becomes

$$\frac{L_I}{L_w}\geqslant 2B^{1/n}\frac{n}{n+1}\int_0^1\tau_s(V_s)\frac{dV_s}{f'(V_s)}+\frac{mg}{Nb\tau_0}. \tag{37}$$

For Robosnail II, the integrals in (37) are particularly simple. The surface velocity, V_s, is roughly constant in the wave region, thus

$$\frac{L_I}{L_w} \geqslant 1 + \left(\frac{n+1}{n}\right)^{2n} \frac{dp}{dx}(1 - Y_+) + \frac{mg}{Nb\tau_0}. \tag{38}$$

In our mechanical crawler, the right-hand side of Eq. (38) can easily become dominated by the weight of the snail if we do not take some care to minimize the weight of the robot components. Since the yield stress of Laponite is only about 100 Pa, Robosnail II was designed to be as light as possible (31.6 g), hence the choice of Nitinol wires rather than an on-board motor.

In optimizing direct wave crawlers, evidently there is a complicated tradeoff between the geometrical design of the foot and rheological properties of the interstitial fluid. The larger the foot speed, the smaller the Bingham number and the higher the shear stress beneath the contraction wave. Thus, one cannot continue to increase the foot speed and the shear stress without eventually allowing the fluid beneath the interwave to yield. Likewise, one loses the anchor of the interwave if one lengthens the contraction region, L_w, too much in maximizing "muscle" area to make V_0 as large as possible. In the limit of larger yield stress (or equivalently, smaller V_s), the mucus exerts less surface shear stress for given foot speed if it is shear thickening ($n > 1$). On the other hand, in the limit of smaller yield stress (larger V_s), it is far more advantageous in this regard if the mucus is shear thinning (see Fig. 6).

Having built two prototypes and demonstrated the feasibility of propelling crawlers using direct and retrograde mechanisms, future studies will turn to the challenge of using the mathematical models to optimize the design of new crawlers. Again, the issues that arise in retrograde versus direct crawlers are radically different. As we have briefly discussed, for retrograde crawlers, an important design focus is likely to be a geometrical optimization problem, namely, to derive optimal designs for the shape of the foot and hence the shape of the traveling wave. In contrast, the optimization of direct wave crawlers relies heavily on optimizing the material properties of the interstitial fluid. An ideal fluid would have a large yield stress to support the weight of the snail and it should have a fast heal time to maximize the velocity of the crawler. As a sample point of reference, we note that the healing time scale for Laponite is on the order of minutes[17] compared to the heal time for pedal mucus, which has evolved to be as fast as 0.1 s.[6] Clearly there is the potential to vastly increase crawling capabilities through design and optimization of synthetic fluids. So far, we have not yet explored the effect of rheology on retrograde crawlers, which is likely to play a role in addition to the geometric considerations outlined above. Both material and geometric optimization questions are topics of current investigation.

ACKNOWLEDGMENTS

This research was partially supported by NSF Grant No. CCF-0323672 and Schlumberger-Doll Research (SDR).

[1] F. Vlès, "Sur les ondes pediuses de Mollosques reptateurs," C. R. Hebd. Seances Acad. Sci. **145**, 276 (1907).
[2] S. Moffett, "Locomotion in the primitive pulmonate snail *Melampus Bidentatus*: Foot structure and function," Biol. Bull. **157**, 306 (1979).
[3] H. W. Lissmann, "The mechanism of locomotion in gastropod molluscs, I. Kinematics," J. Exp. Biol. **21**, 58 (1945).
[4] M. W. Denny, "A quantitative model for the adhesive locomotion of the terrestrial slug *Ariolimax columbianus*," J. Exp. Biol. **91**, 195 (1981).
[5] H. W. Lissmann, "The mechanism of locomotion of gastropod molluscs, II. Kinetics," J. Exp. Biol. **22**, 37 (1946).
[6] M. Denny, "The role of gastropod pedal mucus in locomotion," Nature (London) **285**, 160 (1980).
[7] A. Ito and H. Yasukawa, "Film structured soft actuator for biomimetics of snail's gastropod locomotion," in The 6th International Conference Control, Automation, Robotics and Vision ICARCV'2000, 2000.
[8] L. Mahadevan, S. Daniel, and M. K. Chaudhury, "Biomimetic ratcheting motion of a soft, slender, sessile gel," Proc. Natl. Acad. Sci. U.S.A. **101**, 23 (2004).
[9] It is interesting to note that a similar force balance in the y direction results in no net lift for a wave that is symmetric about the trough, despite experimental evidence to the contrary. This puzzle and various resolutions are discussed in more detail in Refs. 10 and 11.
[10] J. Ashmore, C. del Pino, and T. Mullin, "Cavitation in a lubrication flow between a moving sphere and a boundary," Phys. Rev. Lett. **94**, 124501 (2005).
[11] J. M. Skotheim and L. Mahadevan, "Soft lubrication," Phys. Rev. Lett. **92**, 245509 (2004).
[12] Hancock proposed a similar mechanism for fully immersed filaments, swimming in a Newtonian fluid, in which a longitudinal compression propagates along the body propelling in the organism forward (Ref. 13).
[13] G. J. Hancock, "The self-propulsion of microscopic organisms through liquids," Proc. R. Soc. London, Ser. A **217**, 96 (1953).
[14] O. Reynolds, "On the theory of lubrication and its applications to Mr. Beauchamp Tower's experiments, including an experimental determination of the viscosity of olive oil," Philos. Trans. R. Soc. London **177**, 157 (1886).
[15] N. J. Balmforth and R. V. Craster, "A consistent thin-layer theory for Bingham plastics," J. Non-Newtonian Fluid Mech. **84**, 65 (1999).
[16] N. Willenbacher, "Unusual thixotropic properties of aqueous dispersions of laponite RD," J. Colloid Interface Sci. **182**, 501 (1996).
[17] B. Abou, D. Bonn, and J. Meunier, "Nonlinear rheology of Laponite suspensions under an external drive," J. Rheol. **47**, 979 (2003).
[18] G. Taylor, "Analysis of the swimming of microscopic organisms," Proc. R. Soc. London, Ser. A **209**, 447 (1951).